Proceedings Paper:
Middlemiss, L.A., Rennie, A.J.R., Sayers, R. et al. (2020) Characterisation of batteries by electrochemical impedance spectroscopy. In: Cruden, A., (ed.) Energy Reports. 4th Annual CDT Conference in Energy Storage and Its Applications, 09-10 Jul 2019, Southampton, UK. Elsevier, pp. 232-241. ISSN: 2352-4847. EISSN: 2352-4847.

https://doi.org/10.1016/j.egyr.2020.03.029

Available online at www.sciencedirect.com
ScienceDirect
Energy Reports 6 (2020) 232–241
www.elsevier.com/locate/egyr

4th Annual CDT Conference in Energy Storage and Its Applications, Professor Andrew Cruden, 2019, 07-19, University of Southampton, U.K.

Characterisation of batteries by electrochemical impedance spectroscopy

Laurence A. Middlemiss[a,*], Anthony J.R. Rennie[b], Ruth Sayers[b], Anthony R. West[a]

[a] *Department of Materials Science and Engineering, The University of Sheffield, Sheffield S1 3JD, UK*
[b] *Faradion Ltd., The Innovation Centre, Sheffield S1 4DP, UK*

Received 28 February 2020; accepted 22 March 2020

Abstract

In the pursuit of batteries with higher energy density and lower cost, central to advancement of the technology is the ability to prolong cycle life. Techniques are sought which can elucidate information on battery degradation without significantly disrupting the performance of cells. Electrochemical impedance spectroscopy (EIS) offers a non-destructive route to in-situ analysis of the dynamic processes occurring inside a battery. The technique is relatively easy to use, but meaningful data analysis requires assignment of spectroscopic features to battery impedance components. Three-electrode cell configurations afford a way to potentially disentangle the impedance components. This paper examines a number of three-electrode cell designs reported in the literature, and compares their advantages and limitations. EIS results obtained using a novel in-house, three-electrode pouch cell are reported and the results compared with those obtained from conventional two-terminal impedance complex plane plots. In this way, the separate contributions of anodic and cathodic impedances can be assessed.

Peer-review under responsibility of the scientific committee of the 4th Annual CDT Conference in Energy Storage and Its Applications, Professor Andrew Cruden, 2019.

Keywords: Batteries; Electrochemical impedance spectroscopy; Three-electrode; Degradation

1. Introduction

A growing global energy demand coupled with a need to mitigate climate change has led to dramatic growth in the deployment of renewable energy technologies [1,2]. An important accompaniment to these is the requirement for a greater amount of energy storage, of which batteries are a major component [3]. A key criterion with respect to rechargeable batteries is cycle life, i.e. how many cycles a battery can undergo before significant loss of performance.

All batteries lose performance on cycling [4]. This can be evaluated using *ex-situ* post-mortem analysis which involves disassembly of cells before analysis of the separated cell components [5]. However, it can be difficult to preserve the various parts of the cell 'intact', without contamination of the materials to be studied; in addition,

* Corresponding author.
E-mail address: lamiddlemiss1@sheffield.ac.uk (L.A. Middlemiss).

https://doi.org/10.1016/j.egyr.2020.03.029

Peer-review under responsibility of the scientific committee of the 4th Annual CDT Conference in Energy Storage and Its Applications, Professor Andrew Cruden, 2019.

destructive testing eradicates the ability to gather information on dynamic processes that occur during battery operation.

Electrochemical impedance spectroscopy (EIS) is a non-destructive technique which provides a considerable amount of information in a relatively short space of time, while preserving integrity of the battery [6]. It allows *in situ* dynamic measurements during battery cycling as well as *ex situ* measurements at various states of charge and discharge. In EIS, a small *ac* signal is applied over a wide frequency range and the response measured. EIS is particularly sensitive to systems that contain several impedance elements, including bulk components and interfaces, which makes it well-suited to study a multi-component device such as a battery. Different components and processes within a cell operate on different timescales, i.e. they have different time constants and can be separated in the frequency domain using EIS.

2. Degradation mechanisms in batteries

All batteries experience reduction in performance with cycling. This can be due to a variety of degradation (ageing) mechanisms, which can be associated with one or more of the components/interfaces of a cell [7]. Degradation leads to decrease in capacity and/or power [8]. For metal-ion batteries, e.g. Li- and Na-ion, degradation pathways can be divided into three possible primary processes [9]:

- Loss of the alkali metal (lithium, sodium)
- Loss of the active cathode/anode material
- Deterioration of ionic transport through components and across interfaces

Loss of the alkali metal component or of the active cathode/anode material results in a drop in capacity, whereas deterioration of ionic transport is detected by a rise in internal cell impedance. Table 1 summarises the major degradation mechanisms that are known to occur in rechargeable metal-ion batteries.

Table 1. Degradation mechanisms in rechargeable metal-ion batteries [7].

Cause	Effect	Result
Electrolyte decomposition	Loss of alkali metal, deterioration of ionic transport	Capacity fade, impedance rise
Solid electrolyte interphase (SEI) formation	Loss of alkali metal, deterioration of ionic transport	Capacity fade, impedance rise
Binder decay	Loss of alkali metal, loss of active electrode material, deterioration of ionic transport	Capacity fade, impedance rise
Particle contact loss	Loss of active electrode material, deterioration of ionic transport	Capacity fade, impedance rise
Particle cracking	Loss of alkali metal, loss of active electrode material	Capacity fade
Metal plating	Loss of alkali metal	Capacity fade
Transition metal dissolution	Loss of active electrode material	Capacity fade
Structural disordering/unfavourable phase transitions	Loss of active electrode material	Capacity fade
Changes in porosity	Deterioration of ionic transport	Impedance rise
Decrease in electrode surface area	Deterioration of ionic transport	Impedance rise
Oxidation of conductive additive	Deterioration of ionic transport	Impedance rise
Current collector corrosion	Deterioration of ionic transport	Impedance rise

3. Methodology

To perform EIS on batteries, a frequency response analyser (FRA) is typically used in combination with an electrochemical interface. The electrochemical interface applies a constant voltage (CV) or constant current (CC) and the FRA superimposes an *ac* signal. A multiplexer connects the FRA to the battery test system. A typical setup is shown in Fig. 1. The battery is connected using four wires — two for current flow and two for cell potential. The FRA outputs a signal to the cell via the counter electrode (I-) and the signal is returned through the working electrode (I+). It also connects to a pair of reference electrode points (V+ and V-) to measure the voltage across the cell.

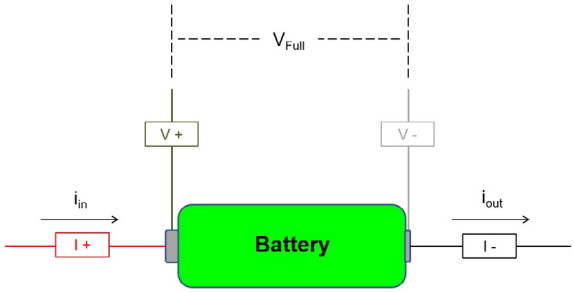

Fig. 1. Wiring configuration for impedance measurement of a battery.

The FRA applies a small *ac* signal, usually in the range mHz–MHz, and measures the response. EIS can be used in either potentiostatic (constant voltage) or galvanostatic (constant current) mode [10]. Potentiostatic mode, where a voltage is applied at each frequency and the resultant current measured, is most common. The current responds at the same frequency as the applied voltage but may be shifted in phase. An important factor is that a reproducible steady state is necessary for valid impedance measurements on a battery [6] since EIS can give inaccurate results on a system that is not at steady state. In order to ensure a steady state, EIS usually is carried out with a small potentiostatic signal amplitude of 10 mV so that the cell response is pseudo-linear (in phase). If the system is non-linear, the response contains harmonics of the input signal frequency. Therefore, in order to accurately perform EIS on a cell during cycling, a 'rest' or open circuit voltage (OCV) period is often applied first so that the cell voltage does not vary significantly during measurements [11]. Similarly, an additional rest period on open circuit is often implemented following the impedance scan to allow the cell to 'recover' from any changes that occur during the EIS run, prior to continuing with constant current/constant voltage (CC/CV) cycling.

4. Analysis of impedance data

EIS may be used to characterise either the static or dynamic impedance of a battery. Regardless of whether galvanostatic or potentiostatic mode is used, the *ac* signal, and therefore the response, is sinusoidal [10]. The impedance, Z, is a frequency-dependent complex number characterised by the ratio of voltage to current and the phase angle shift between them, Φ.

$$Z = \frac{V}{I} = Z_0 e^{j\Phi} = Z_0\,(cos\,\Phi + j sin\,\Phi) = Z' + jZ'' \quad \text{where } j = \sqrt{-1} \tag{1}$$

A generated impedance spectrum consists of resistive and reactive components. The resistance is made up of a combination of electronic and ionic resistances. The most common form of plotting impedance data is as a Z^* complex plane plot of Z'' against Z' on linear scales, also known as a Nyquist plot. Presenting data in this way displays the resistance along the (real) x-axis and reactance (including capacitance) along the (imaginary) y-axis.

While EIS is relatively easy to use, the difficulty often lies in data interpretation since Z^* plots generally consist of a small number of often poorly-resolved arcs. Models are used in the form of equivalent electrical circuits, comprised of resistance, R, and capacitance, C, elements, together with constant phase elements, CPE, to represent departures from ideality, with the objective of assigning these to different physical processes and components within the battery.

An idealised spectrum that may represent a multicomponent system, such as a metal-ion battery, is shown in Fig. 2 together with an equivalent circuit that contains four components. There is also often a tail below the real Z' axis at higher frequencies, not shown, which is due to inductive effects associated with the battery and/or the experimental setup. With decreasing frequency, the first feature is a non-zero ohmic resistance where the spectrum intersects the real Z' axis at high frequency; it is represented in the equivalent circuit by a resistor (R_{HF}). The two semi-circles, usually of different size, are each represented by a resistor and capacitor in parallel (known as a parallel RC element). To account for, and model, a non-ideal or distorted semi-circle, a constant phase element (CPE), which is a combined variable resistor and variable capacitor, is added in parallel with the parallel RC element. The impedance of a constant phase element is defined as:

$$Z^* = \frac{1}{(j\omega)^n Y_0} \tag{2}$$

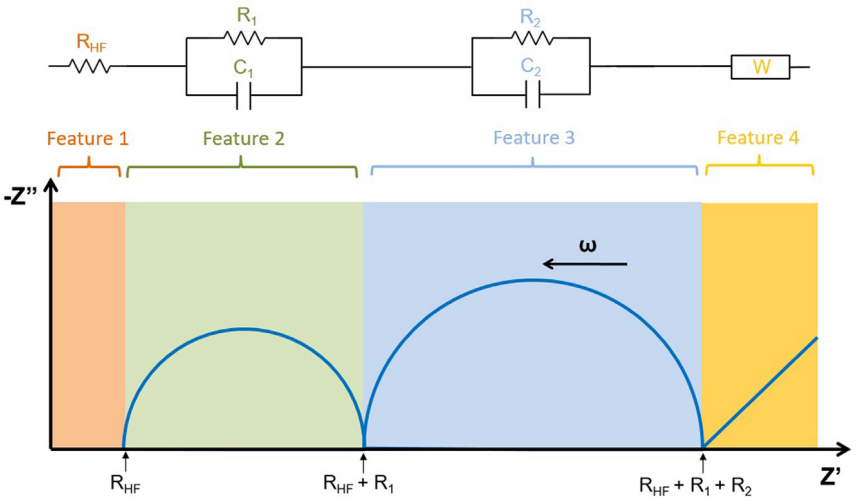

Fig. 2. Schematic idealised impedance complex plane plot for a multicomponent system together with its ideal equivalent electrical circuit.

where Y_0 is a constant, the angular frequency (ω) is given by $\omega = 2\pi f$ and $0 < n < 1$. The exponent n is responsible for the depression of the semi-circle. For a value $n = 1$ the CPE reduces to a perfect capacitor, and for $n = 0$ it is a resistor [12]. The fourth feature, at low frequency, is frequently an inclined spike, which can be a non-ideal capacitor represented by a CPE or a Warburg element (where $n = 0.5$) if the spike is at 45° to the Z' axis. [13]. The physical significance of a Warburg element is a diffusion-controlled process which adds an additional impedance to the overall response [14,15].

5. Three-electrode arrangements

One limitation to analysing two-terminal EIS data is that it can often be difficult to deconvolute impedance components that have similar time constants (RC products) [16]. Half-cell measurements can be used to study separately the impedances associated with the two electrodes but may not reflect the processes occurring in a full-cell battery at different states of charge and discharge [17]. Measurements may also be made on symmetrical cells [18,19] in which the two cells are disassembled and the cathode of one is replaced with the anode of the other, and vice versa. However, such approaches are limited as symmetrical cells cannot be charged and discharged in the same way as a fully functioning battery. The arduous process of disassembling and reassembling cells must therefore be carried out repeatedly, in order to gather information at different states of charge and states of health.

A three-electrode cell design [20] incorporates a spectator reference electrode, which does not interfere with the cycling of the battery. The battery is then charged/discharged as usual, but as well as recording the impedance across the entire cell, the impedances of the cathode and anode can be measured separately against the reference. It is therefore possible to monitor how each electrode contributes to the overall impedance of the battery. Three-electrode measurements may suffer from measurement artefacts associated with distortions caused by electrical/electrochemical and geometrical asymmetry in the experimental setup [21]. Geometrical asymmetry is created by misalignment of positive and negative electrodes. Electrochemical asymmetry is due to different kinetics at each electrode [22]. Electrode polarisation processes possess different time constants and their impedances change differently with frequency. Both geometrical and electrochemical asymmetries lead to an inhomogeneous electrolyte current density at the reference electrode, which may be responsible for distortions in the measured impedance spectra [23]. Care must be taken therefore to ensure that the design of the battery does not affect the cell performance and electrode impedances [24]. To check the validity of an experimental setup, the individual impedances of the cathode and anode can be added and the combined spectra compared with the impedance of the full-cell [25].

A number of different three-electrode configurations for lithium-ion batteries have been reported [26–28] using a variety of cell configurations and different reference electrodes [29]. The reference electrode needs to maintain a stable potential under prolonged and extensive testing and not interfere with the normal cell operation [30]. The

reference electrode should be non-polarisable and have a low internal resistance [27,29]. For lithium-ion batteries, either Li metal or a Li-containing compound are the most popular.

The shape and position of the reference electrode may also affect the impedance results [22], as well as the geometry of the cell setup and location of the reference electrode [24]. The most popular geometries are point- [31], wire- [32] or ring-type [33]. A point-type reference electrode is a small piece of, say, Li metal for Li-ion batteries, which is placed away from the centre of the cell. A wire-type reference is similar to the point-type but extends within the electrolyte into the centre of the cell. A ring-type, often utilised in coin cells, surrounds the centre of the battery. Some of these are displayed in Fig. 3 [23,24,34].

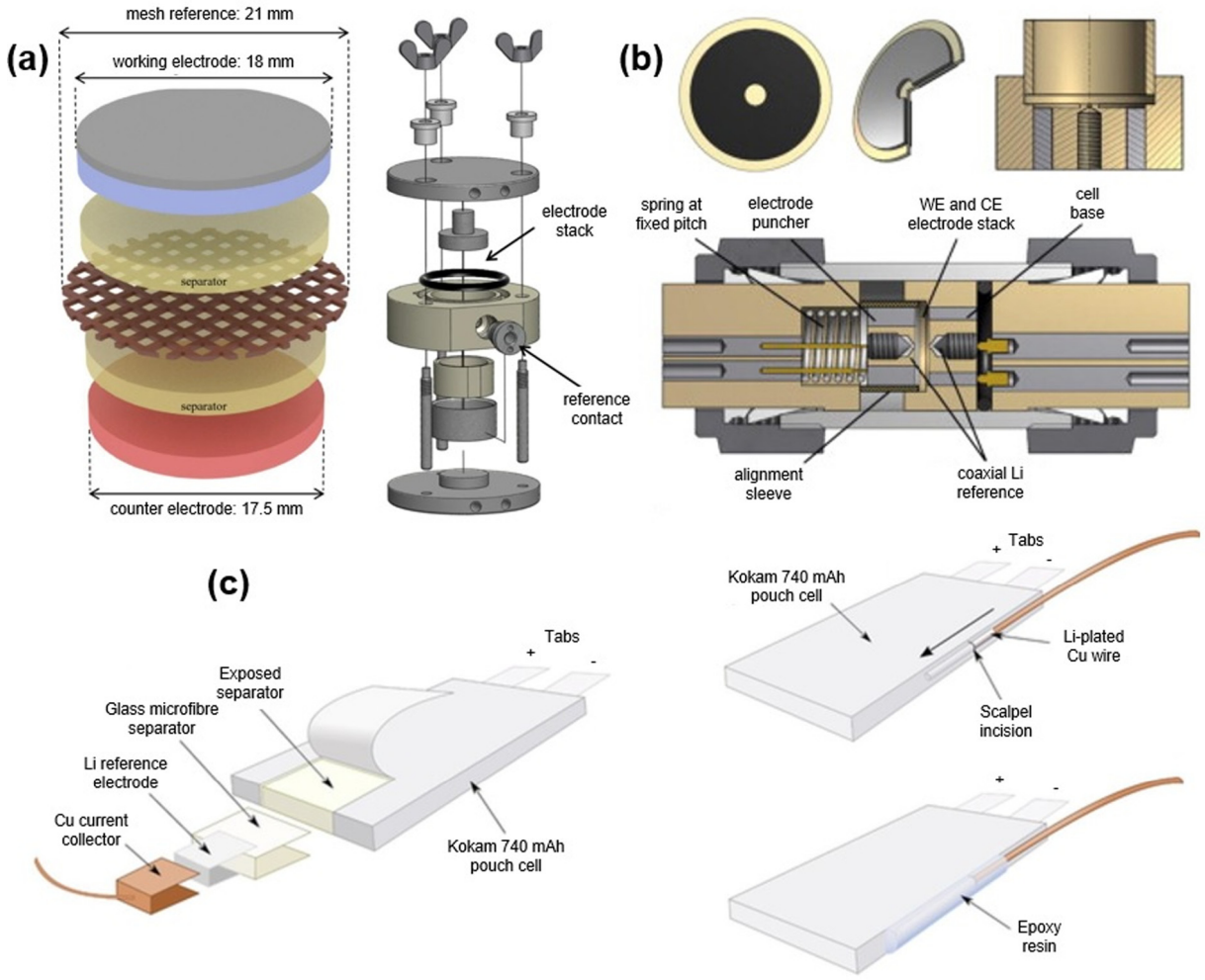

Fig. 3. Some of the different three-electrode cell designs: (a) coin cell, where a mesh reference electrode is placed between two separators [23]; (b) coaxial cell developed from a modified Swagelok [24]; (c) commercial pouch cells retrofitted with a third reference electrode [34]. *Source:* Adapted from references [23,24,34].

The coin cell in (a) used a bespoke mesh reference electrode, in place of a more conventional type [23]. The electrochemical and geometrical asymmetries are then negligible because the mesh is efficient at measuring the potential between the electrodes, where the current distribution is homogeneous. However, the greater surface area of the mesh creates multiple transport paths which leads to an additional polarisation process within the cell and can cause distortions at certain frequencies. The design in (b) was developed to overcome limitations with the imprecise electrode alignment and an asymmetric reference electrode geometry of Swagelok cells [24]. Typically, in a three-electrode Swagelok cell (also known as a T-cell), the reference electrode contacts the electrolyte/separator at its outer rim. The reference voltage is susceptible to fluctuation under changing current, such as during impedance

measurements, and can lead to a distortion of data: artificial loops are often seen in the impedance response. In the design used by these authors [24], the reference electrode is moved to a coaxial position in combination with precise alignment of the electrode stack. This led to improved performance, but the measurements were still limited, particularly in the high frequency region. In design (c) a commercial pouch cell was retrofitted with a reference electrode using two different methods: "patch" and "wire" [34]. The "patch" method lead to significant disruption in the battery structure and to deterioration in cell performance. However, the "wire" method, where a Li-plated Cu wire was inserted down one side of the pouch, gave a performance close to that of a conventional two-electrode cell in terms of capacity and voltage. This design was not utilised for EIS measurements.

6. Results and discussion

An in-house three-electrode pouch cell configuration (Fig. 4) was developed with the reference electrode sandwiched between two separators. Cells were assembled in an argon-filled glove box. The composite electrodes consist of the active material component, which was mixed with a binder and carbon black conductive additive. Slurries were formed and drawn down onto carbon-coated Al current collector foil. The separators were soaked in liquid electrolyte prior to cell assembly. Impedance measurements were performed using a potentiostat with a parallel FRA. Impedance was measured by applying an *ac* potential between two electrodes and measuring the resulting current (potentiostatic mode). Three EIS scans were made using different methods for connecting the testing equipment to the electrodes: (i) the impedance was measured without using the reference electrode (full cell measurement); (ii) the impedance of the cathode was measured against the reference electrode; (iii) the anode was measured versus the reference electrode. The cells were cycled under constant current (CC) between 1 and 4.2 V, using 14 mA g^{-1} on charging and 28 mA g^{-1} on discharging. A constant voltage (CV) step was applied at the top of charge until the current dropped below 2.8 mA g^{-1} in order to maximise the capacity obtained from the batteries. Four additional hours allowed equilibration after each charging/discharging step before performing EIS. An additional one-hour open circuit voltage (OCV) hold after EIS allowed the cell to return to a steady state, prior to continuing with the CC/CV run.

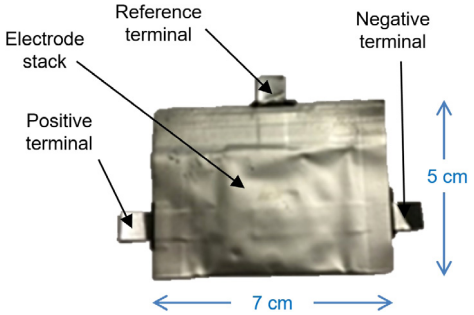

Fig. 4. The 10 mAh three-electrode pouch cell used in this study. The reference electrode sits at the top and is sandwiched between two separators, with the cathode and anode either side, inside the cell.

Whereas impedance measurements have been performed extensively in the past on lithium-ion batteries [35,36], and several different three-electrode cell designs developed [23,24,34], a similar amount of research has not yet been reported on Na-ion technology. Fig. 5 shows EIS data (0.01–100,000 Hz) for a two-electrode ∼10 mAh sodium-ion (Na-ion) battery. This pouch cell consists of the same design as in Fig. 4, but without the presence of a spectator reference electrode. The impedance scan was performed across the entire cell between the positive and the negative electrodes. The cathode (positive electrode) was a layered sodium transition metal oxide, the anode (negative electrode) a non-graphitisable hard carbon, and the electrolyte a sodium salt dissolved in a mixed carbonate solvent. The spectra presented in Fig. 5 were not corrected for geometry of the various cell components. Raw data were collected after the Na-ion battery was discharged for the first time (at 0% state of charge).

The complex plane plot for the full-cell in (a) shows a high-frequency arc with non-zero high frequency intercept and a larger low-frequency distorted (broadened) semi-circle. To a first approximation, the equivalent electrical circuit for this Na-ion battery consists of two parallel RC elements and a resistor connected in series. Hence, there

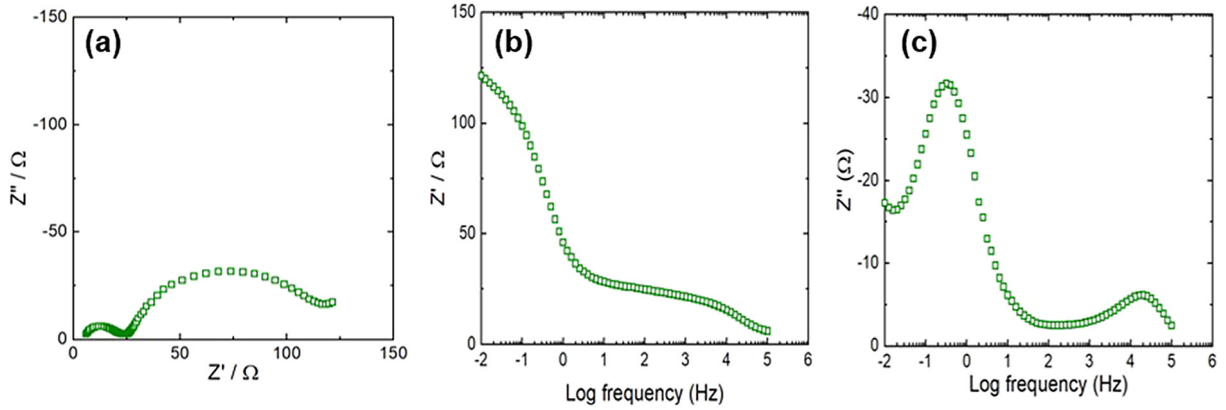

Fig. 5. Some two-electrode EIS data for an in-house constructed fully discharged sodium-ion battery: (a) impedance complex plane plots, spectroscopic plots of Z'(b), and Z'' (c).

are at least three resistive components with values roughly 5 (R_{HF}), 20 (R_1) and 90 (R_2) Ω. The most common form of plotting impedance data for analysis is in the form of Z'' plotted against Z' on linear scales, also known as a Nyquist plot, as seen in (a). Data can alternatively be presented as a spectroscopic Z' plot in (b) and Z'' plot in (c), which allows separate visualisation of the Z', Z'' components against frequency on a logarithmic scale.

Fig. 6 shows EIS data (10 mHz–1 MHz) for a three-electrode ∼10 mAh Na-ion cell after it was discharged for the first time (at 0% state of charge). The impedance complex plane plots in Fig. 6(a) show full-cell (black), cathode (red) and anode (blue) data sets, with respective total impedances of ∼115, ∼75 and ∼40 Ω respectively. The total resistance for the full-cell equals the sum of those for the cathode and the anode, as shown by the pink data and, therefore, no corrections to the generated impedance spectra were needed. The absence of such a requirement suggests that the three-electrode pouch cell configuration used here affords a superior measurement to many of the previous cell designs. Furthermore, it can be seen that these impedance plots look very similar to the two-electrode ones in Fig. 5, which means that introduction of a reference electrode does not cause the impedance results to differ from what is seen inside a regular two-electrode cell. Hence, using this setup, it is possible to extract meaningful results from EIS measurements performed on three-electrode cells and make interpretations that can be applied to commercially-relevant two-electrode batteries.

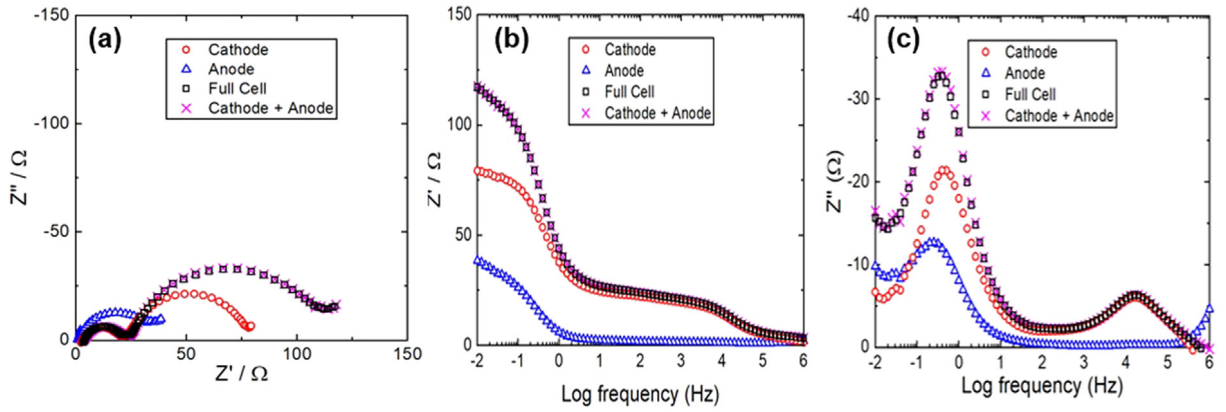

Fig. 6. Some three-electrode EIS data for an in-house constructed sodium-ion battery: (a) impedance complex plane plots, spectroscopic plots of Z'(b), and Z'' (c).

The shape of the Nyquist plots (a) for the cathode and full-cell, in the three-electrode measurement, are similar to one another, but that for the anode is quite different, appearing to consist of just one arc. While the cathode and full-cell data closely resemble each other at high frequency, there is much greater disparity at low frequency.

This is demonstrated more clearly by the spectroscopic Z' (b) and Z'' (c) plots. The key point is that the anode shows a Z'' peak at a similar frequency to the cathode (c), both of which, therefore, contribute to the low frequency semicircle for the full cell in (a). However, the high frequency peak in the cathode Z'' plot (c) has no comparable peak in the anode response and the cathode is responsible entirely for the high frequency semicircle in the full cell data (a). Previous studies in the literature have rarely utilised different ways of presenting impedance data, such as Z' and Z'' spectroscopic plots, thus constraining the interpretation of results.

Separate measurements performed on the conductivity of the liquid electrolyte [37] indicated that the combined resistance of this and the separators is likely to be responsible for the high frequency intercept, R_{HF}. The origin of the other two resistive components, R_1 and R_2, is currently under investigation. These results are similar to those seen with lithium-ion batteries that have a dominant cathode impedance [38]; however, there are also noticeable differences, such as the anode making a more significant contribution to the impedance of the battery in the data shown here.

The observed anodic resistance may be associated with formation of a solid electrolyte interphase on the surface of the anode, which is reported to behave differently to those seen in Li-ion batteries [39]. Further work is currently underway using different cell configurations, more in-depth analysis of the impedance data to elucidate the origins of the different resistive components, and analysis of impedance data recorded at different states of charge/discharge. It is anticipated that this research should help identify the major degradation mechanisms in the sodium-ion batteries studied here.

7. Conclusions

EIS is a powerful in-situ non-destructive technique for monitoring the impedances inside a battery and how they may change at different stages during battery cycling [40]. More extended analysis of impedance data can provide significantly more insight than obtained by using complex plane plots alone. In order to maximise the technique fully, a three-electrode setup is required so that the impedance contributions at each electrode can be separated and characterised.

A novel in-house three-electrode cell has been built and tested in this work. It eliminates the need for any data correction and appears to afford superior measurements to many of the cell designs reported in the literature. Data obtained on a prototype sodium-ion battery using this cell and technique show that the cathode contributes at least two components to the overall resistance of the cell whereas the anode contributes a single major component. Work is ongoing using different cell designs and more in-depth analysis to elucidate the origins of the different individual resistive components. It is anticipated that this research should have important consequences for optimising and extending the cycle life of new battery systems.

Declaration of competing interest

The authors declare that they have no known competing financial interests or personal relationships that could have appeared to influence the work reported in this paper.

Acknowledgement

We thank the EPSRC under grant EP/L016818/1 for a Ph.D. studentship for L. Middlemiss.

References

[1] Ellabban O, Abu-Rub H, Blaabjerg F. Renewable energy resources: current status, future prospects and their enabling technology. Renew Sustain Energy Rev 2014;39:748–64.
[2] Edenhofer O, Pichs-Madruga R, Sokona Y, editors. Renewable energy sources and climate change mitigation : special report of the intergovernmental panel on climate change. New York: Cambridge University Press.; 2015.
[3] Larcher D, Tarascon J-M. Towards greener and more sustainable batteries for electrical energy storage. Nature Chem 2015;7(1):19–29.
[4] Palacín MR, de Guibert A. Why do batteries fail? Science 2016;351(6273):1253292.
[5] Waldmann T, Iturrondobeitia A, Kasper M, Ghanbari N, Aguesse F, Bekaert E, Daniel L, Genies S, Gordon IJ, Löble W, De Vito E, Wohlfahrt-Mehrens M. Post-mortem analysis of aged lithium-ion batteries: disassembly methodology and physico-chemical analysis techniques. J Electrochem Soc 2016;163(10):2149–64.
[6] Tröltzsch U, Kanoun O, Tränkler H-R. Characterizing aging effects of lithium ion batteries by impedance spectroscopy. Electrochim Acta 2006;51(8–9):1664–72.

[7] Vetter J, Novák P, MR, Wagner, Veit C, Möller K-C, Besenhard M. Winter JO, Wohlfahrt-Mehrens M, Vogler C, Hammouche A. Ageing mechanisms in lithium-ion batteries. J Power Sources 2005;147(1-2):269–81.
[8] Wright RB, Christophersen JP, Motloch CG, Ho CD, Battaglia VS, Barnes JA, Duong TQ, Sutula RA. Power fade and capacity fade resulting from cycle-life testing of advanced technology development program lithium-ion batteries. J Power Sources 2003;119:865–9.
[9] Kindermann FM, Keil J, Frank A, Jossen A. A SEI modeling approach distinguishing between capacity and power fade. J Electrochem Soc 2017;164(12):E287–94.
[10] Huet F. A review of impedance measurements for determination of the state-of-charge or state-of-health of secondary batteries. J Power Sources 1998;70(1):59–69.
[11] Bundy K, Karlsson M, Lindbergh G, Lundqvist A. An electrochemical impedance spectroscopy method for prediction of the state of charge of a nickel-metal hydride battery at open circuit and during discharge. J Power Sources 1998;72(2):118–25.
[12] Barsoukov E, Macdonald JR. Impedance spectroscopy : theory, experiment, and applications. second ed. Hoboken: John Wiley & Sons; 2005.
[13] Rodrigues S, Munichandraiah N, Shukla AK. AC Impedance and state-of-charge analysis of a sealed lithium-ion rechargeable battery. J Solid State Electrochem 1999;3(7–8):397–405.
[14] Levi MD, Aurbach D. Simultaneous measurements and modeling of the electrochemical impedance and the cyclic voltammetric characteristics of graphite electrodes doped with lithium. J Phys Chem B 1997;101(23):4630–40.
[15] Levi MD, Aurbach D. Diffusion coefficients of lithium ions during intercalation into graphite derived from the simultaneous measurements and modeling of electrochemical impedance and potentiostatic intermittent titration characteristics of thin graphite electrodes. J Phys Chem B 1997;101(23):4641–7.
[16] Li J, Murphy E, Winnick J, Kohl PA. Studies on the cycle life of commercial lithium ion batteries during rapid charge–discharge cycling. J Power Sources 2001;102(1–2):294–301.
[17] Song JY, Lee HH, Wang YY, Wan CC. Two- and three-electrode impedance spectroscopy of lithium-ion batteries. J Power Sources 2002;111(2):255–67.
[18] Chen CH, Liu J, Amine K. Symmetric cell approach and impedance spectroscopy of high power lithium-ion batteries. J Power Sources 2001;96(2):321–8.
[19] Momma T, Yokoshima T, Nara H, Gima Y, Osaka T. Distinction of impedance responses of Li-ion batteries for individual electrodes using symmetric cells. Electrochim Acta 2014;131:195–201.
[20] Nagasubramanian G. Two-and three-electrode impedance studies on 18650 Li-ion cells. J. Power Sources 2000;87(1–2):226–9.
[21] Ender M, Illig J, Ivers-Tiffée E. Three-electrode setups for lithium-ion batteries. J Electrochem Soc 2017;164(2):A71–9.
[22] Ender M, Weber A, Ivers-Tiffée E. Analysis of three-electrode setups for AC-impedance measurements on lithium-ion cells by FEM simulations. J Electrochem Soc 2012;159(2):A128.
[23] Costard J, Ender M, Weiss M, Ivers-Tiffée E. Three-electrode setups for lithium-ion batteries. J Electrochem Soc 2017;164(2):A80–7.
[24] Klink S, Madej E, Ventosa E, Lindner A, Schuhmann W, La Mantia F. The importance of cell geometry for electrochemical impedance spectroscopy in three-electrode lithium ion battery test cells. Electrochem Commun 2012;22:120–3.
[25] Hsieh G, Ford SJ, Masona TO, Pedersonb LR. Experimental limitations in impedance spectroscopy: part I - simulation of reference electrode artifacts in three-point measurements. Solid State Ion 1996;91(3–4):191–201.
[26] Blyr A, Sigala C, Amatucci G, Guyornard D, Chabre Y, Tarascon J-M. Cells in their discharged state understanding by means of three-electrode measurements. J Electrochem Soc 1998;145(1):194–209.
[27] Bünzli C, Kaiser H, Novák P. Important aspects for reliable electrochemical impedance spectroscopy measurements of Li-ion battery electrodes. J Electrochem Soc 2015;162(1):A218–22.
[28] Beattie SD, Loveridge MJ, Lain MJ, Ferrari S, Polzin BJ, Bhagat R, Dashwood R. Understanding capacity fade in silicon based electrodes for lithium-ion batteries using three electrode cells and upper cut-off voltage studies. J Power Sources 2016;302:426–30.
[29] Raccichini R, Amores M, Hinds G. Critical review of the use of reference electrodes in Li-ion batteries: a diagnostic perspective. Batteries 2019;5(1):12.
[30] Dollé ML, Orsini F, Gozdz AS, Tarascon J-M. Development of reliable three-electrode impedance measurements in plastic Li-ion batteries. J Electrochem Soc 2001;148(8):A851–7.
[31] Hoshi Y, Narita Y, Honda K, Ohtaki T, Shitanda I, Itagaki M. Optimization of reference electrode position in a three-electrode cell for impedance measurements in lithium-ion rechargeable battery by finite element method. J Power Sources 2015;288(2015):168–75.
[32] Landesfeind J, Pritzl D, Gasteiger HA. An analysis protocol for three-electrode Li-ion battery impedance spectra: part I. Analysis of a high-voltage positive electrode. J Electrochem Soc 2017;164(7):A1773–83.
[33] Itagaki M, Honda K, Hoshi Y, Shitanda I. In-situ EIS to determine impedance spectra of lithium-ion rechargeable batteries during charge and discharge cycle. J Electroanal Chem 2015;737(15):78–84.
[34] McTurk E, Birkl CR, Roberts MR, Howey DA, Bruce PG. Minimally invasive insertion of reference electrodes into commercial lithium-ion pouch cells. ECS Electrochem Lett 2015;4(12):A145–7.
[35] Andre D, Meiler M, Steiner K, Wimmer C, Soczka-Guth T, Sauer DU. Characterization of high-power lithium-ion batteries by electrochemical impedance spectroscopy. I. Experimental investigation. J Power Sources 2011;196(12):5334–41.
[36] Andre D, Meiler M, Steiner K, Walz H, Soczka-Guth T, Sauer DU. Characterization of high-power lithium-ion batteries by electrochemical impedance spectroscopy. ii: modelling. J Power Sources 2011;196(12):5349–56.
[37] Middlemiss LA. [Ph.D. thesis], Sheffield: The University of Sheffield; 2020.

[38] Amine K, Chen CH, Liu J, Hammond M, Jansen A, Dees D, Bloom I, Vissers D, Henriksen G. Factors responsible for impedance rise in high power lithium ion batteries. J Power Sources 2001;97–98:684–7.

[39] Mogensen R, Brandell D, Younesi R. Solubility of the solid electrolyte interphase (SEI) in sodium ion batteries. ACS Energy Lett 2016;1(6):1173–8.

[40] Gordon IAJ, Grugeon S, Takenouti H, Tribollet B, Armand M, Davoisne C, Debart A, Laruelle S. Electrochemical impedance spectroscopy response study of a commercial graphite-based negative electrode for li-ion batteries as function of the cell state of charge and ageing. Electrochim Acta 2017;223:63–73.